DR. YOUNGRYEL RYU (Orcid ID: 0000-0001-6238-2479)

Article type : Primary Research Articles

Inconsistencies of interannual variability and trends in long-term satellite leaf area index products

Chongya Jiang¹, Youngryel Ryu^{1,2,3,4*}, Hongliang Fang^{5,6}, Ranga Myneni⁷, Martin Claverie^{8,9}, Zaichun Zhu¹⁰

¹Brain Korea 21 Plus Team, Seoul National University, Seoul, Republic of Korea

²Department of Landscape Architecture and Rural Systems Engineering, Seoul National University, Seoul, Republic of Korea

³Interdisciplinary Program in Agricultural and Forest Meteorology, Seoul National University, Republic of Korea

⁴Interdisciplinary Program in Landscape Architecture, Seoul National University, Republic of Korea

⁵LREIS, Institute of Geographic Sciences and Natural Resources Research, Chinese Academy of Sciences, Beijing, China

⁶University of Chinese Academy of Sciences, China

⁷Department of Earth and Environment, Boston University, Boston, Massachusetts, USA

⁸Department of Geographical Sciences, University of Maryland, College Park, Maryland,

USA

⁹NASA Goddard Space Flight Center, Greenbelt, Maryland, USA

This article has been accepted for publication and undergone full peer review but has not been through the copyediting, typesetting, pagination and proofreading process, which may lead to differences between this version and the Version of Record. Please cite this article as doi: 10.1111/gcb.13787

¹⁰Sino-French Institute for Earth System Science, College of Urban and Environmental Sciences, Peking University, Beijing, China

*Corresponding author:

Youngryel Ryu

Department of Landscape Architecture and Rural Systems Engineering, Seoul National

University, Seoul 151-921, Republic of Korea

Phone: 82-2-880-4871, Fax: 82-2-873-5113

Email: yryu@snu.ac.kr

Intended for Global Change Biology

Abstract

Understanding the long-term performance of global satellite leaf area index (LAI) products is important for global change research. However, few effort has been devoted to evaluating the long-term time series consistencies of LAI products. This study compared four long-term LAI products (GLASS, GLOBMAP, LAI3g, and TCDR) in terms of trends, interannual variabilities and uncertainty variations from 1982 through 2011. This study also used four ancillary LAI products (GEOV1, MERIS, MODIS C5, and MODIS C6) from 2003 through 2011 to help clarify the performances of the four long-term LAI products. In general, there were marked discrepancies between the four long-term LAI products. During the pre-MODIS period (1982–1999), both linear trends and interannual variabilities of global mean LAI followed the order GLASS>LAI3g>TCDR>GLOBMAP. The GLASS linear trend and interannual variability were almost 4.5 times those of GLOBMAP. During the overlap period

(2003–2011), GLASS and GLOBMAP exhibited a decreasing trend, TCDR no trend, and LAI3g an increasing trend. GEOV1, MERIS, and MODIS C6 also exhibited an increasing trend, but to a much smaller extent than that from LAI3g. During both periods, the R² of detrended anomalies between the four long-term LAI products were smaller than 0.4 for most regions. Interannual variabilities of the four long-term LAI products were considerably different over the two periods, and the differences followed the order GLASS>LAI3g> TCDR>GLOBMAP. Uncertainty variations quantified by a collocation error model followed the same order. Our results indicate that the four long-term LAI products were neither intraconsistent over time nor inter-consistent with each other. These inconsistencies may be due to NOAA satellite orbit changes and MODIS sensor degradation. Caution should be used in the interpretation of global changes derived from the four long-term LAI products.

Key words: GLASS, GLOBMAP, intercomparison, LAI3g, leaf area index (LAI), TCDR, time series

Introduction

Leaf area index (LAI), indicating the area of green leaves per unit of ground surface area, is identified as an essential climate variable (ECV) by the Global Climate Observing System (GCOS) (Gobron & Verstraete, 2009). The acquisition of reliable global LAI data is a prerequisite for modeling, mapping, and monitoring land surface ecosystems (Sellers *et al.*, 1995; Asner *et al.*, 2003; Ryu *et al.*, 2011). Recently, several long-term (≥30 years) global LAI products have been produced (Liu *et al.*, 2012; Zhu *et al.*, 2013; Claverie *et al.*, 2016; Xiao *et al.*, 2016). These long-term products are of great importance in understanding the

responses and feedback of land surface ecosystems to climate changes, elevated CO₂ concentrations, and anthropogenic activities (Piao *et al.*, 2015; Mao *et al.*, 2016; Zhu *et al.*, 2016).

Appropriate use of global satellite LAI products requires comprehensive evaluation studies. To address this issue, the Committee on Earth Observation Satellites (CEOS) Land Product Validation (LPV) subgroup proposed a four-stage validation hierarchy (Morisette *et al.*, 2006). Under this framework, both theoretical and physical uncertainties of global satellite LAI products have been investigated (Fang *et al.*, 2012a, 2012b), against a target accuracy requirements of $\pm 20\%$ proposed by GCOS (GCOS, 2011). However, most existing evaluation studies focused on fine-resolution (≤ 1 km) and short-term (e.g., since the 2000s) LAI products, in terms of absolute magnitude (Garrigues *et al.*, 2008), spatial pattern (Fang *et al.*, 2013), and seasonal trajectory (Verger *et al.*, 2016). In comparison, less effort has been devoted from a long-term perspective (i.e., since the 1980s).

Long-term global satellite LAI products are derived from Advanced Very High Resolution Radiometer (AVHRR) datasets on board of the National Oceanic and Atmospheric Administration (NOAA) satellite series, which are prone to larger uncertainties than short-term datasets (Guay *et al.*, 2014; Tian *et al.*, 2015). Sources of uncertainty in AVHRR time series data mainly involve sensor degradation, lack of onboard calibration, drift of satellite orbits, and changes in platforms and sensors (Tucker *et al.*, 2005; Pinzon & Tucker, 2014). These data source uncertainties are likely to propagate to LAI products, along with additional uncertainties caused by algorithms. Platform-related uncertainties may vary gradually or abruptly, and, therefore the performances of LAI products and other downstream products, such as gross primary productivity (GPP), may also vary over time. To meet the needs of

global climate studies, GCOS has proposed guidelines requiring a stability of $\pm 10\%$ for LAI products (GCOS, 2011). Therefore, evaluating global satellite LAI products from a long-term perspective is of great importance to ensure their correct application in global change research.

Trends and interannual variabilities in terrestrial ecosystems are two overarching issues that long-term LAI products should address. Many studies have reported a greening earth related to global warming and elevated CO₂ concentration (Fensholt & Proud, 2012; Myneni et al., 1997) and oscillations caused by El Niño and other extreme events (de Jong et al., 2012; Myneni et al., 1998), based on analyses of long-term Normalized Difference Vegetation Index (NDVI) products. LAI has an advantage over NDVI due to its explicit ecological meaning, so that global long-term satellite LAI products have been considered as references to interpret LAI time series simulated by land surface models (Lucht *et al.*, 2002; Piao *et al.*, 2006; Mao *et al.*, 2013). However, the degrees of trends and interannual variabilities are uncertain because the agreements and discrepancies between different long-term LAI products are unclear.

The present study was performed to undertake a detailed evaluation on the consistencies of four long-term global satellite LAI products (Table 1): Global Land Surface Satellite (GLASS) (Xiao *et al.*, 2016); GLOBMAP (Liu *et al.*, 2012); LAI3g (Zhu *et al.*, 2013); and Terrestrial Climate Data Record (TCDR) (Claverie *et al.*, 2016). Aiming at this goal, we examined their trends, interannual variabilities, and uncertainty variations. We also compared the four long-term LAI products with other widely used but short-term products: GEOV1 (Baret *et al.*, 2013); MERIS (Tum *et al.*, 2016); MODIS Collection 5 (C5) (Shabanov *et al.*,

2005); and MODIS Collection 6 (C6) (Yan et al., 2016). Consequently, three time periods were investigated separately: 30-year long-term period (1982–2011), pre-MODIS period (1982–1999) and overlap period (2003 – 2011). We address a single question: are current long-term LAI products intra-consistent (having comparable spatiotemporal patterns itself over different time periods) and inter-consistent (having comparable spatiotemporal patterns with each other)?

Materials and Methods

Long-term LAI products from 1982–2015

GLASS LAI product

GLASS product (version 03), acquired from ftp://ftp.glcf.umd.edu/, is generated every 8 days, using 0.05° resolution NOAA/AVHRR surface reflectance datasets provided by NASA's Long Term Data Record (LTDR) project before 2001 (Pedelty *et al.*, 2007), and 1 km resolution Terra/MODIS surface reflectance datasets (MOD09) since 2001 (Xiao *et al.*, 2016). The algorithm fuses Terra/MODIS LAI (MOD15) with clump-corrected CYCLOPES LAI, and establishes relationships between the fused LAI dataset and NOAA/AVHRR or Terra/MODIS surface reflectance over Benchmark Land Multisite Analysis and Intercomparison of Products (BELMANIP) sites using biome-specific general regression neural networks (Xiao *et al.*, 2016). Yearly reflectance-LAI pairs are used to train the neural networks and estimate LAI time series (Xiao *et al.*, 2014).

GLOBMAP LAI product

GLOBMAP product (version 01), acquired from http://www.globalmapping.org/, is generated in 1/13.75° spatial resolution, using biweekly NDVI provided by the Global Inventory Modeling and Mapping Studies (GIMMS) before March 2000 (Tucker *et al.*, 2005), and 8-day Terra/MODIS surface reflectance (MOD09) since March 2000. The algorithm inverses a geometrical optical model to generate MODIS LAI from MOD09 data since March 2000, and then establishes pixel-based relationships between MODIS LAI and simple ratio (SR) vegetation index derived from GIMMS NDVI during the overlapping period from 2000 to 2006. Such relationships are finally used to derive LAI from AVHRR SR before March 2000 (Liu *et al.*, 2012).

LAI3g LAI product

LAI3g product (version 01), acquired from http://sites.bu.edu/cliveg/datacodes/, is generated biweekly in 1/12° spatial resolution (Zhu *et al.*, 2013). The input data is the third—generation NDVI (NDVI3g) provided by GIMMS. The algorithm is based on feed-forward neural networks connecting the MODIS LAI Beijing Normal University (BNU) version (Yuan et al., 2011) to NDVI3g. This calibration procedure is conducted on multi-year average monthly LAI and NDVI data, so that 12 neural networks are involved, one for each month. The calibrated neural networks are further used to retrieve AVHRR LAI from NDVI3g.

TCDR product

AVHRR TCDR product (version 04), acquired from ftp://eclipse.ncdc.noaa.gov/, is provided every day in 0.05° spatial resolution (Claverie *et al.*, 2016). The product is mainly derived from a surface reflectance dataset obtained by NOAA/AVHRR sensors, which has been

geolocated, calibrated, cloud and snow removed, and corrected for atmospheric and bidirectional reflectance distribution function (BRDF) effects (Vermote *et al.*, 2009). The algorithm is based on an artificial neural network connecting Terra + Aqua combined MODIS LAI (MCD15) to AVHRR TCDR reflectance separately for five biomes (Claverie *et al.*, 2016). The calibration procedure is conducted using data over BELMANIP2 sites, and the calibrated neural network is further used to retrieve AVHRR LAI from TCDR reflectance.

Ancillary LAI products from 1999–2015

GEOV1 LAI product

GEOV1 LAI product, acquired from http://land.copernicus.eu/, is generated every 10 days in 1/112° spatial resolution. MODIS and CYCLOPES LAI products are fused to generate the "best estimates" of LAI using a linear formula (Baret *et al.*, 2013). A neural network is trained between the fused LAI and the SPOT/VEGETATION top of canopy directionally normalized reflectance values over the global BELMANIP sites (Baret *et al.*, 2006). The trained neural network provides LAI estimates from the SPOT/VEGETATION reflectance.

MERIS LAI product

MERIS LAI product, acquired from https://centaurus.caf.dlr.de:8443/, is generated every 10 days in 1/360° spatial resolution (Tum *et al.*, 2016). The algorithm is based on the training of a neural network over a database of simulated top-of-atmosphere radiances, using a coupled leaf-canopy-atmosphere radiative transfer model (Bacour *et al.*, 2006). The trained neural network is used to estimate LAI from ENVISAT/MERIS L1B observations at 15 spectral

bands. A harmonic analysis is further incorporated into the algorithm to fill data gaps caused by irregular sampling strategy of MERIS full-resolution (FR) data.

MODIS C5 and C6 LAI products

MODIS LAI products, acquired from ftp://ladsweb.nascom.nasa.gov, are generated every 8 days in 1 km and 500 m spatial resolution, for MOD15A2 C5 and MOD15A2H C6, respectively. The main algorithm employs biome-specific look-up tables (LUTs) simulated from a 3D radiative transfer model to search for LAI values for a specific set of sun-object-sensor geometries, and observed red and near-infrared reflectances from Terra/MODIS C5 and C6 reflectance, respectively (Huang et al., 2008; Knyazikhin et al., 1998; Yan et al., 2016). When the main algorithm fails, a backup algorithm based on the LAI–NDVI relationships derived from model simulations is used for LAI estimation (Myneni et al., 1997). A major improvement in MODIS C6 LAI product is the usage of MOD09GA C6 reflectance product, which applies a new sensor calibration.

Data processing and analysis

Calculation of global mean LAI

We obtained annual LAI maps and global mean LAI time series from each LAI product. Monthly mean 0.5° LAI was calculated by averaging LAI values from original spatiotemporal resolution. The residual data gaps were filled by a widely used Harmonic ANalysis of Time Series (HANTS) method, which applies a least squares curve fitting procedure for time series signals based on harmonic components of periodic functions (Roerink *et al.*, 2000; Zhou *et al.*, 2015). We calculated annual growing season mean LAI maps by averaging monthly LAI values with monthly mean temperature higher than 0°C

(Fig. S1) (Prentice *et al.*, 2011). Monthly averaged daily mean temperatures (1982–2015) were obtained from the Climatic Research Unit (CRU) high-resolution gridded datasets (version 3.24) (Harris *et al.*, 2014), and we calculated multi-year averaged monthly mean temperatures to ensure that the same growing season land mask was used over the entire period (1982–2015) across different products (Fig. S2). The global mean LAI values were calculated by area-weighted average over annual growing season mean LAI maps excluding unvegetated regions (Fig. S3).

Time-series analysis

We used an Ensemble Empirical Mode Decomposition (EEMD) method along with the classical linear model method to detect LAI trend. The EEMD method decomposes time series into a group of oscillatory components at different frequency levels without any predetermined basis functions (Huang et al., 1998), and EEMD is its enhanced version overcoming the scale mixing problem (Wang, 2009). The number of components usually varies from three to eight, depending on the length of the time series (Huang et al., 2003), In this study, we decomposed the long-term and ancillary LAI products into four and three components, respectively. Summing different components generates adaptive trends at different temporal scales (Ji et al., 2014). We summed the last two components to account for decadal-scale trends according to Wu et al. (2007). Annual anomalies were obtained by subtracting adaptive trends from the original time series, and the standard deviation of each detrended anomaly was calculated as a quantitative metric of the interannual variability. Linear trends and interannual variabilities were also calculated pixel-by-pixel to generate spatial patterns.

We used a collocation error model to quantify uncertainty time series of LAI products. The triple collocation error model (TCEM) is the primary implementation of the collocation model, which obtains analytical solutions of random errors of three spatially and temporally collocated remote sensing products with no need for a "true" observation (Stoffelen, 1998; Gruber *et al.*, 2016). We extended the original TCEM to a general collocation error model (GCEM) so that more than three collocated datasets can be involved. For *m* collocated datasets, \mathbf{x}_i (i = 1, 2, ..., m), the covariance between each pair of datasets, including intra-pair cases, is given by (McColl *et al.*, 2014):

$$Cov(\mathbf{x}_i, \mathbf{x}_i) = \theta_i \theta_i + Cov(\mathbf{\varepsilon}_i, \mathbf{\varepsilon}_i)$$
(1)

where $\mathbf{\varepsilon}_i$ is the random error of \mathbf{x}_i , θ_i is a parameter related to system error of \mathbf{x}_i and the variation of hypothetical truth, and $\text{Cov}(\mathbf{\varepsilon}_i, \mathbf{\varepsilon}_j) = 0$ when $i \neq j$ according to the independent error assumption (McColl *et al.*, 2014). A total of m(m+1)/2 equations can be obtained, along with 2m unknown parameters, i.e., θ_i and σ_i (i = 1, 2, ..., m) where $\sigma_i^2 = \text{Cov}(\mathbf{\varepsilon}_i, \mathbf{\varepsilon}_i)$ and σ_i is taken as uncertainty. When $m \geq 3$ GCEM is a well-constrained and solvable system, and a numerical solution can be achieved using the least squares technique (Pan *et al.*, 2015). In this study, pixels over one land cover type in a continent constituted sampling of \mathbf{x}_i and yielded one regional uncertainty estimate. The land cover type was derived from the global land cover product for the year 2000 (GLC2000) (Bartholomé & Belward, 2005; Giri *et al.*, 2005) (Fig. S3). Regions with less than 60 pixels were masked to avoid numerical problems caused by inadequate sampling of \mathbf{x}_i (Fang et al., 2012). Global LAI uncertainty was calculated yearly as the sum of regional uncertainties, weighted by the area of each region. We used a $2\times$ standard deviation of each uncertainty time series, corresponding to 95% range of variations assuming an approximately normal distribution, as the quantitative metric of the

temporal uncertainty variation. Relative uncertainty and relative uncertainty variation were also calculated, using LAI value as a normalization factor according to GCOS (2011).

Results

Linear trends

Global mean LAI values generally varied within the range of 1.55±0.3 according to the four long-term and four ancillary LAI products (Fig. 1). The long-term products showed higher global mean LAI values than ancillary products after 2001, with GLOBMAP as an exception that showed the lowest values. The largest differences appeared in 2011, when LAI3g was 45% higher than GLOBMAP, 30% higher than MODIS C5, and 25% higher than MODIS C6. The global mean values for TCDR, GLASS, and LAI3g differed from each other before 1995 but became similar after 2001.

The linear trends of the four long-term LAI products varied substantially (Fig. 1 and Table 2). Over the 30 years (1982–2011), GLASS, LAI3g, and TCDR showed significant increasing trends, while GLOBMAP showed a significant decreasing trend. The mean trend of these four products was about 0.053 m² m⁻² decade⁻¹, with a coefficient of variation of 119%. Particularly, the difference between GLASS and GLOBMAP reached 0.154 m² m⁻² decade⁻¹. There were notable differences between 1982–1999 and 2003–2007. GLASS and GLOBMAP changed from significant increasing trends (0.115 and 0.026 m² m⁻² decade⁻¹, respectively) to significant decreasing trends (-0.044 and -0.098 m² m⁻² decade⁻¹,

respectively). LAI3g maintained a significant increasing trend but its slope value almost doubled ($0.082~\text{m}^2~\text{m}^{-2}$ decade⁻¹ for 1982-1999 and 0.151 for 2003-2007). TCDR changed from a significant increasing trend ($0.057~\text{m}^2~\text{m}^{-2}$ decade⁻¹) during 1982-1999 to an insignificant trend ($0.004~\text{m}^2~\text{m}^{-2}$ decade⁻¹) during 2003-2007. While the four long-term LAI products disagreed in trend signs and values during the overlap period (2003-2011), the three ancillary LAI products, GEOV1, MERIS, and MODIS C6, agreed very well, with a mean trend ($0.056~\text{m}^2~\text{m}^{-2}$ decade⁻¹ ± 2 SD) ranged about $0.028 \sim 0.084~\text{m}^2~\text{m}^{-2}$ decade⁻¹ (Fig. 1 and Table 2). However, the trend values from the four long-term LAI products all fell far out of this range. It is also noted that MODIS C5 had a small decreasing trend (p > 0.05), whereas MODIS C6 had an increasing trend (p < 0.05).

Spatial patterns of linear trends of the four long-term LAI product showed some similarities during 1982 – 1999 (Fig. 2a-d). GLASS, LAI3g, and TCDR revealed a greening earth as around 45% of vegetated land surface area showed an increasing trend, especially in the northern high latitudes. GLOBMAP also showed an increasing trend over those areas. However, it is notable that agreements among these products were limited in trend signs. GLASS exhibited the largest trend values, followed by LAI3g and TCDR, while GLOBMAP exhibited much smaller trends.

Spatial patterns of linear trends of the four long-term LAI product showed large discrepancies during 2003 – 2011 (Fig. 2e-h). More than 20% GLASS and GLOBMAP but only <10% LAI3g and TCDR showed browning of the vegetated land surface in tropical forests, North America, and Central Russia. Only about 10% GLASS, GLOBMAP, and TCDR but 33% LAI3g showed a greening tendency in the Northern Hemisphere. On contrast, the ancillary

GEOV1, MERIS, and MODIS C6 showed quite similar values, with 15–20% positive trend and about 5% negative. Regions with growing LAI included Eastern Siberia, Europe, Eastern China, India, Eastern Australia, and Southern Africa.

Adaptive trends, detrended anomalies and interannual variabilities

The EEMD method detected decadal-scale adaptive trends and various temporal patterns were demonstrated for the four long-term LAI products over the three decades examined (Fig. 3a). In the first decade (1982–1991), both GLOBMAP and LAI3g showed slight increasing trends, GLASS showed a slight decrease trend, and TCDR showed a flat tendency. During the second decade (1992–2001), GLASS, TCDR and LAI3g showed overall increasing trend to different degrees, whereas GLOBMAP shows a flat tendency. During the third decade (2002–2011), both GLOBMAP and GLASS showed decreasing trends, LAI3g showed an increasing trend, and TCDR showed a flat tendency. The three ancillary LAI products, GEOV1, MERIS, and MODIS C6, all showed increasing trends, but a clear turning point was observed for GEOV1 around 2003 when its platform changed from SPOT4 to SPOT5. In contrast to MODIS C6, MODIS C5 showed an overall flat tendency.

Diverse patterns of global mean LAI anomalies were observed after removing the adaptive trends (Fig. 3b and Table 2). The most distinct feature was the presence of a dividing point around 2001. Before 2001, there were considerable oscillations in anomalies of global mean LAI curves, and the amplitudes differed from each other. During the pre-MODIS period (1982–1999), the mean interannual variability of the four long-term LAI products was 0.044

m² m⁻² year⁻¹, with a coefficient of variation of 61%. Particularly, the interannual variability of GLASS was 4.4 times that of GLOBMAP. During 2003–2011, the four long-term LAI products showed much smaller variations than those before 2001, with a mean±SD about 0.013±0.001 m² m⁻² year⁻¹. The four ancillary LAI products also showed a small mean interannual variability of 0.010 m² m⁻² year⁻¹ with a standard deviation of 0.003 m² m⁻² year⁻¹, both of which were comparable with those of the four long-term LAI products.

Different LAI products showed different spatial patterns of interannual variability during 1982 – 1999 (Fig. 4a-d). The tropical forests showed markedly large discrepancies. GLASS, LAI3g, TCDR and GLOBMAP exhibited > 0.20, 0.15 – 0.20, 0.10 – 0.15, and < 0.15 m² m⁻² year⁻¹ interannual variability values in most tropical forest areas, respectively. In temperate forests similar discrepancies were observed, that GLASS exhibited the largest interannual variabilities, followed by LAI3g and TCDR, while GLOBMAP exhibited much smaller interannual variabilities.

Spatial patterns of interannual variabilities of the four long-term LAI product showed some similarities during 2003 – 2011 (Fig. 4e-h). Hotspots were usually observed in tropical forests, Eastern South America, Central Eurasia, Eastern Siberia, and Eastern Australia. These regions were also highlighted in three ancillary LAI products, GEOV1, MODIS C5 and MODIS C6.

Uncertainties and changes in uncertainty

Fig. 5 showed the global uncertainties and relative uncertainties for the four long-term LAI products and three ancillary LAI products. MODIS C5 was excluded because its error was likely to be highly correlated with MODIS C6, violating the assumption of in the collocation model. All seven datasets were characterized by an uncertainty <0.3 on an annual scale. During 1982–2011, the mean global relative uncertainties followed the order LAI3g (8.5%) < GLASS (11.7%) < TCDR (13.0%) < GLOBMAP (19.6%) (Table 2). These statistics were comparable to the ancillary LAI products, with the order GEOV1 (6.4%) < MODIS C6 (13.6%) < MERIS (14.0%). Pre-MODIS (1982–2001) and overlap (2003–2011) periods showed only slight differences for GLOBAMP, LAI3g, and TCDR. In contrast, GLASS showed a notable decrease in 2001, resulting in the largest relative uncertainty variation (3.5%), while those of the other three LAI products were not larger than 2.0%.

The average maps of annual growing season mean LAI uncertainties and relative uncertainties were shown in Fig. 6. The spatial pattern of uncertainty was generally in accordance with the distribution of LAI (Fig. 6a). Tropical evergreen broadleaf forest regions showed the highest uncertainties (>0.40). Intermediate uncertainty values (0.20–0.30) were found for the subtropical and boreal forest regions. Uncertainties were low (<0.15) over sparsely vegetated areas. Conversely (Fig. 6b), low LAI regions including high latitude areas, Western America, Central Asia, Sub-Saharan Africa, Southern South America, Southern Africa, and Central and Western Australia generally showed large relative uncertainties (>20%). The relative uncertainties for forest regions varied between 10% and 20%. The spatial pattern of uncertainty variation was similar to the uncertainty map (Fig. 7a), with high LAI regions showing larger variations over the 30-year period. Tropical forest regions showed the largest variations (>0.10), followed by subtropical and boreal forests (0.05–0.10). Meanwhile,

the relative uncertainty variation showed similar spatial patterns to the relative uncertainty (Fig. 7b), with large relative uncertainty variation mainly appearing in shrublands and grasslands.

Discussion

Are current long-term LAI products intra-consistent over time?

This study revealed the intra-inconsistency of the four long-term LAI products from two aspects: changes in interannual variability between two periods (1982 – 1999 and 2003 – 2011) and uncertainty variation over the 30-year period (1982 – 2011).

Remarkably different annual anomaly oscillations were observed before and after 2001 (Fig. 3b). Such pronounced differences were not observed from other long-term datasets related to LAI, such as solar radiation (Sanchez-Lorenzo *et al.*, 2015), temperature and precipitation (Yan et al., 2013), and CO₂ growth and carbon sink (Keenan *et al.*, 2016). With the assumption that interannual variability was constant over the 30 years, we could use the ratio of interannual variability during 1982–1999 to that during 2003–2011 as an intra-consistency index. A larger deviation away from 1 would indicate a greater degree of intra-inconsistency. Fig. 8a showed that the global ratio followed the order GLOBMAP (1.2) <TCDR (2.1) < LAI3g (4.3) <GLASS (6.7), indicating the order of intra-inconsistency at global scale. The most significant intra-inconsistency appeared in tropical evergreen broadleaf forests (Fig. 4a-d against Fig. 4e-h), where the intra-inconsistency index of TCDR, LAI3g and GLASS were in range of 6–12 (Fig. 8a). High latitude (such as boreal evergreen needleleaf forests) and arid

(such as woody savannas and grasslands) regions generally showed relatively low (< 4) intrainconsistency (Fig. 8a).

Fig. 5 showed small and stable uncertainties and relative uncertainties of global annual growing season mean LAI for different products over the 30 years. Statistics listed in Tables 2 showed that for all four long-term LAI products, the mean relative uncertainties were smaller than the 20% target accuracy and the relative uncertainty variations were smaller than the 10% target stability proposed by GCOS (GCOS, 2011). However, we were unable to deduce they satisfied the requirements for accuracy or stability, because the definitions in GCOS resemble both systematic error and random error, while uncertainty estimated from collocation error model approximates the latter (Fang et al., 2012). Instead, considering the unreasonably large oscillations before 2001 (Fig. 3b), we might infer substantial relative uncertainty variations, i.e., instability, of systematic error component which were not captured by those of random error used in this study. We also noted that even relative uncertainty variation of random errors were highly correlated with the intra-inconsistency index (Fig. 8a), indicating the same order of intra-inconsistency index at global scale: GLOBMAP (1.1%) < TCDR (1.6%) < LAI3g (2.0%) < GLASS (3.5%). Differing from intrainconsistency index, sparsely vegetated areas tended to have larger relative uncertainty variations as mean LAI was used as a normalization factor.

Satellite platform changes were likely a main reason for such intra-inconsistencies. GLASS exhibited the most significant change in 2001 because of the change in satellite platform from NOAA/AVHRR to Terra/MODIS (Fig. 3). NOAA/AVHRR itself was also multi-platform, composed of seven satellites and two sensors (AVHRR2 on board NOAA 07, 09, 11, and 14,

and AVHRR3 on board NOAA 16, 18, and 19). This might have caused the intrainconsistency issue for LAI3g and TCDR to some extent. A satellite change also caused an
abrupt change in the GEOV1 time series in 2003 (Fensholt *et al.*, 2009). Although
GLOBMAP changed its platform in 2000 as well, it has exhibited relative good intraconsistency. This might be related to its special LAI retrieval algorithm, which divides the
input into 10 bins, with SR-LAI relationship built within each bin. Such discretization
strategy had been shown to be effective for improving the quality of retrievals from lowquality inputs and improving temporal smoothness (Liu *et al.*, 2012). Cloudiness was another
potential factor influencing year-to-year variations, especially for tropical evergreen forests
which contribute most to global LAI interannual variabilility (Samanta *et al.*, 2010).
However, such difference was unlikely to cause decadal level difference (the difference
between 1982 – 1999 and 2003 – 2011) as long as the use same cloud masking technique was
used over the period.

Are current long-term LAI products inter-consistent with each other?

This study revealed the inter-inconsistency of the four long-term LAI products from discrepancies in trend and interannual variability for both global values and spatial patterns.

Greening or browning is a basic question of global change research (Myneni *et al.*, 1997a; Zhu *et al.*, 2017), and the four long-term LAI products yielded different answers as different adaptive trend patterns were shown (Fig. 3a). While adaptive trends revealed intrinsic properties of data associated with time scales, piecewise linear trends still provided intuitive

quantitative intercomparison (Table 2). During the pre-MODIS period (1982–1999), all of the four long-term LAI products collectively detected the global greening trend (Fig. 1), especially contributed by the widespread greening trends in the Northern Hemisphere (Fig. 9a). However, their linear trends disagreed with each other in the following order: GLOBMAP (0.026 m² m²² decade⁻¹)<TCDR (0.057)<LAI3g (0.082)<GLASS (0.115), and the linear trend maps showed generally different values between each other (Fig. 2a-d). Note the global trends followed the same order as product intra-consistency. During the overlap period (2003–2011), the four long-term LAI products displayed different global trends, that browning trends by GLASS and GLOBMAP, no trend by TCDR, and greening trend by LAI3g (Fig. 1). Spatially, discrepancies in trend signs mainly appeared in tropical forests and temperate forests in Southeastern United States (Fig. 9b and Fig. 2e-h). In contrast, the three ancillary LAI products, GEOV1, MERIS, and MODIS C6 showed good agreements on trends both globally and spatially (Fig. 1 and Fig. 2i-l).

Assessing environmental controls on vegetation variability is another essential issue in global change research (Seddon *et al.*, 2016; Jung *et al.*, 2017), and the four long-term LAI products yielded considerably different annual anomalies (Fig. 3b). During the pre-MODIS period (1982–1999), the interannual variability values followed the order GLOBMAP (0.017 m² m⁻² year⁻¹) < TCDR (0.027) < LAI3g (0.057) < GLASS (0.074). Note this was same as the order of the product intra-consistency. Additionally, the agreement on spatial variations of annual anomalies was low, as was illustrated in Fig. 10. About 76% and 60% of pixels showed mean R² < 0.40, and relatively higher R² values were mainly observed in sparsely vegetated regions. Densely-vegetated regions with high interannual variability but low correlation might be a severe problem for application. Recent studies indicated that a variety of remote sensing models could only explain less than 40% interannual variability of gross primary productivity

(GPP) (Yuan *et al.*, 2014; Jiang & Ryu, 2016). We inferred that LAI or equivalent input data, such as fraction of photosynthetically active radiation (FPAR), may limit the capacity of remote sensing models to reliably capture interannual variability of GPP. We further noted that linear trend was highly correlated with interannual variability during the pre-MODIS period (Fig. 8b). This indicated that inconsistency of interannual variability was coupled with that of linear trend, except for boreal evergreen needleleaf forest.

The inter-inconsistency between LAI products were attributed to different methods of treating the satellite orbit change and sensor degradation issues. During the pre-MODIS period (1982-1999), different AVHRR data sources were used to generate the four LAI products: GLASS used LTDR reflectance data; GLOBMAP used GIMMS NDVI data; LAI3g used GIMMS NDVI3g data. TCDR LAI used TCDR reflectance data. The major difference between LTDR and TCDR reflectance was that the latter normalized reflectance at nadir view and 45° solar zenith angle (Claverie et al., 2016), while the former did not apply bidirectional reflectance distribution function (BRDF) correction (Pedelty et al., 2007). The major difference between GIMMS NDVI and NDVI3g was that the former applied the EMD method to minimize varying solar zenith angle effects introduced by orbital drift (Tucker et al., 2005), while the latter placed more emphasis on among-instrument AVHRR calibration (Pinzon & Tucker, 2014). Marked differences between GIMMS NDVI and NDVI3g were also reported by Guay et al. (2014). With the fact that GLASS had much larger interannual variability than TCDR, and LAI3g had much larger interannual variability than GLOBMAP, we inferred that the BRDF effect on AVHRR data could cause exaggerated annual oscillation and consequently unrealistically large interannual variability in LAI products. Because there was a clear linear relationship between linear trend values and interannual variability values during this period (Fig. 8b), we hypothesized that the BRDF effect caused by orbit change

was also related to the trend inconsistency of the four long-term LAI products. However, further investigation is needed to evaluate this hypothesis. During the overlap period, both GLASS and GLOBMAP used MODIS reflectance data as input and they exhibited opposite linear trends to LAI3g and TCDR. This may be because both GLASS and GLOBMAP used MODIS C5 reflectance, which suffered from sensor degradation problems over the past decade (Wang *et al.*, 2012). Such negative bias caused by sensor degradation also propagated to the MODIS C5 LAI product (Fig. 1), which has also been reported in other studies (Yan et al., 2016). Because sophisticated calibration procedure has been applied on MODIS C6 reflectance (Zhang *et al.*, 2017), and therefore the MODIS C6 LAI product has already remedied this issue by using corrected reflectance data (Fig. 1), we suggest that the LAI product teams should also update their products using MODIS C6 reflectance or NDVI.

Suggestions for the usage of current long-term LAI products

According to the uncertainty variation over the 30 years and the ratio of interannual variability during 1982–1999 to that during 2003–2011, GLOBMAP was the most intraconsistent product, followed by TCDR and LAI3g, whereas GLASS was the most inconsistent. Pronounced inconsistency was identified between these LAI products, and both linear trend and interannual variability during pre-MODIS period (1982–1999) were correlated to intra-consistency. However, recommendation of best LAI product during that period could not be drawn. Because scarce long-term continuous field LAI measurements were available before 2000, it was impractical to evaluate annual trends and anomalies of the four long-term LAI products through direct validation using ground data. Further evaluations are still needed through indirect comparisons with climate data and land surface model

simulations. Therefore, we suggest careful usage of current long-term LAI products. A single product or even ensemble of the four products may not be directly considered as relevant references when interpreting long-term global carbon and water cycle studies during pre-MODIS period (1982 – 1999), except for several consensus: 1) trend signs, 2) interannual variability values in high latitude regions, and 3) annual anomalies in arid regions. During overlapped period (2003–2011), none of the four long-term LAI products agree well with the three reference LAI products (GEOV1, MERIS, and MODIS C6) in term of trend, but their interannual variabilities are relatively consistent with each other.

Acknowledgements

This research was funded by the National Research Foundation of Korea (NRF-2014R1A2A1A11051134). H. F. was supported by the National Key Research and Development Program of China (2016YFA0600201). We thank GLCF (http://glcf.umd.edu/), Global mapping (http://www.globalmapping.org/), CLIVEG (http://cliveg.bu.edu/), NCDC (https://www.ncdc.noaa.gov/), Copernicus (http://www.copernicus.eu/), EOC (https://geoservice.dlr.de/web/), and LAADS (https://ladsweb.nascom.nasa.gov/) teams who facilitated the distribution of GLASS, GLOBMAP, LAI3g, TCDR, GEOV1, MERIS, and MODIS global satellite LAI products. The authors declare no conflict of interest. English proofread was supported by Research Institute of Agriculture and Life Sciences at Seoul National University.

References

Asner G, Scurlock J, Hicke J (2003) Global synthesis of leaf area index observations: implications for ecological and remote sensing studies. *Global Ecology & Biogeography*, **12**, 191–205.

Bacour C, Baret F, Béal D, Weiss M, Pavageau K (2006) Neural network estimation of LAI, fAPAR, fCover and LAI×Cab, from top of canopy MERIS reflectance data: Principles and validation. *Remote Sensing of Environment*, **105**, 313–325.

Baret F, Morissette JT, Fernandes R a. et al. (2006) Evaluation of the representativeness of networks of sites for the global validation and intercomparison of land biophysical products: Proposition of the CEOS-BELMANIP. *IEEE Transactions on Geoscience and Remote Sensing*, **44**, 1794–1802.

Baret F, Weiss M, Lacaze R, Camacho F, Makhmara H, Pacholcyzk P, Smets B (2013)

GEOV1: LAI and FAPAR essential climate variables and FCOVER global time series capitalizing over existing products. Part1: Principles of development and production.

Remote Sensing of Environment, 137, 299–309.

Bartholomé E, Belward A (2005) GLC2000: a new approach to global land cover mapping from Earth observation data. *International Journal of Remote Sensing*, **26**, 1959–1977.

Claverie M, Matthews J, Vermote E, Justice C (2016) A 30+ year AVHRR LAI and FAPAR climate data record: Algorithm description and validation. *Remote Sensing*, **8**, 1–12.

Fang H, Wei S, Jiang C, Scipal K (2012a) Theoretical uncertainty analysis of global MODIS, CYCLOPES, and GLOBCARBON LAI products using a triple collocation method.

*Remote Sensing of Environment, 124, 610–621.

- Fang H, Wei S, Liang S (2012b) Validation of MODIS and CYCLOPES LAI products using global field measurement data. *Remote Sensing of Environment*, **119**, 43–54.
- Fang H, Jiang C, Li W et al. (2013) Characterization and intercomparison of global moderate resolution leaf area index (LAI) products: Analysis of climatologies and theoretical uncertainties. *Journal of Geophysical Research: Biogeosciences*, **118**, 529–548.
- Fensholt R, Proud S (2012) Evaluation of Earth Observation based global long term vegetation trends Comparing GIMMS and MODIS global NDVI time series. *Remote Sensing of Environment*, **119**, 131–147.
- Fensholt R, Rasmussen K, Nielsen T, Mbow C (2009) Evaluation of earth observation based long term vegetation trends Intercomparing NDVI time series trend analysis consistency of Sahel from AVHRR GIMMS, Terra MODIS and SPOT VGT data.

 *Remote Sensing of Environment, 113, 1886–1898.
- Garrigues S, Lacaze R, Baret F et al. (2008) Validation and intercomparison of global Leaf
 Area Index products derived from remote sensing data. *Journal of Geophysical*Research: Biogeosciences, 113, G02028.
- GCOS (2011) Systematic observation requirements for satellite-based data products for climate, Supplemental details to the satellite-based component of the "Implementation Plan for the Global Observing System for Climate in Support of the UNFCCC."

 Reference Number GCOS-154, 127 pp.
- Giri C, Zhu Z, Reed B (2005) A comparative analysis of the Global Land Cover 2000 and MODIS land cover data sets. *Remote Sensing of Environment*, **94**, 123–132.
- Gobron N, Verstraete M (2009) Assessment of the status of the development of standards for the Terrestrial Essential Climate Variables: Leaf Area Index (LAI). Global Terrestrial

Observing System, Rome, 12 pp.

- Gruber A, Su C-H, Zwieback S, Crow W, Dorigo W, Wagner W (2016) Recent advances in (soil moisture) triple collocation analysis. *International Journal of Applied Earth Observation and Geoinformation*, **45**, 200–211.
- Guay K, Beck P, Berner L, Goetz S, Baccini A, Buermann W (2014) Vegetation productivity patterns at high northern latitudes: A multi-sensor satellite data assessment. *Global Change Biology*, **20**, 3147–3158.
- Harris I, Jones PD, Osborn TJ, Lister DH (2014) Updated high-resolution grids of monthly climatic observations the CRU TS3.10 Dataset. *International Journal of Climatology*, **34**, 623–642.
- Huang N, Shen Z, Long S et al. (1998) The empirical mode decomposition and the Hilbert spectrum for nonlinear and non-stationary time series analysis. *Proceedings of the Royal Society of London. Series A, Mathematical and Physical Sciences*, **454**, 903–995.
- Huang N, Wu M-L, Long S, Shen S, Qu W, Gloersen P, Fan K (2003) A confidence limit for the empirical mode decomposition and Hilbert spectral analysis. *Proceedings of the Royal Society of London A: Mathematical, Physical and Engineering Sciences*, 459.
- Huang D, Knyazikhin Y, Wang W et al. (2008) Stochastic transport theory for investigating the three-dimensional canopy structure from space measurements. *Remote Sensing of Environment*, **112**, 35–50.
- Ji F, Wu Z, Huang J, Chassignet EP (2014) Evolution of land surface air temperature trend.

 Nature Climate Change, 4, 462–466.
- Jiang C, Ryu Y (2016) Multi-scale evaluation of global gross primary productivity and

evapotranspiration products derived from Breathing Earth System Simulator (BESS). *Remote Sensing of Environment*, **186**, 528–547.

- de Jong R, Verbesselt J, Schaepman ME, de Bruin S (2012) Trend changes in global greening and browning: Contribution of short-term trends to longer-term change. *Global Change Biology*, **18**, 642–655.
- Jung M, Reichstein M, Schwalm CR, Huntingford C, Sitch S (2017) Compensatory water effects link yearly global land CO2 sink changes to temperature. *Nature*, (**In Press**).
- Keenan T, Prentice IC, Canadell J, Williams C, Wang H, Raupach M, Collatz J (2016)

 Recent pause in the growth rate of atmospheric CO2 due to enhanced terrestrial carbon uptake. *Nature Communications*, **7**, 1–9.
- Knyazikhin Y, Martonchik J, Myneni R, Diner D, Running S (1998) Synergistic algorithm for estimating vegetation canopy leaf area index and fraction of absorbed photosynthetically active radiation from MODIS and MISR data. *Journal of Geophysical Research*, **103**, 32257–32276.
- Liu Y, Liu R, Chen JM (2012) Retrospective retrieval of long-term consistent global leaf area index (1981-2011) from combined AVHRR and MODIS data. *Journal of Geophysical Research: Biogeosciences*, **117**, G04003.
- Lucht W, Prentice IC, Myneni R et al. (2002) Climatic control of the high-latitude vegetation greening trend and Pinatubo effect. *Science*, **296**, 1687–1689.
- Mao J, Shi X, Thornton P, Hoffman F, Zhu Z, Myneni R (2013) Global Latitudinal-Asymmetric Vegetation Growth Trends and Their Driving Mechanisms: 1982–2009.

 Remote Sensing, 5, 1484–1497.

- Mao J, Ribes A, Yan B et al. (2016) Human-induced greening of the northern extratropical land surface. *Nature Climate Change*, **6**, 959–963.
- McColl K, Vogelzang J, Konings A, Entekhabi D, Piles M, Stoffelen A (2014) Extended triple collocation: Estimating errors and correlation coefficients with respect to an unknown target. *Geophysical Research Letters*, **41**, 6229–6236.
- Morisette J, Baret F, Privette J et al. (2006) Validation of global moderate-resolution LAI products: A framework proposed within the CEOS land product validation subgroup. *IEEE Transactions on Geoscience and Remote Sensing*, **44**, 1804–1814.
- Myneni R, Keeling C, Tucker C, Asrar G, Nemani R (1997a) Increased plant growth in the northern high latitudes from 1981 to 1991. *Nature*, **386**, 698–702.
- Myneni R, Nemani R, Running S (1997b) Estimation of global leaf area index and absorbed par using radiative transfer models. *Geoscience and Remote Sensing, IEEE Transactions on*, **35**, 1380–1393.
- Myneni R, Tucker C, Asrar G, Keeling C (1998) Interannual variations in satellite-sensed vegetation index data from 1981 to 1991. *Journal of Geophysical Research:***Atmospheres*, 103, 6145–6160.
- Pan M, Fisher C, Chaney N et al. (2015) Triple collocation: Beyond three estimates and separation of structural/non-structural errors. *Remote Sensing of Environment*, **171**, 299–310.
- Pedelty J, Devadiga S, Masuoka E et al. (2007) Generating a long-term land data record from the AVHRR and MODIS Instruments. In: 2007 IEEE International Geoscience and Remote Sensing Symposium, pp. 1021–1025. IEEE.

- Piao S, Friedlingstein P, Ciais P, Zhou L, Chen A (2006) Effect of climate and CO2 changes on the greening of the Northern Hemisphere over the past two decades. *Geophysical Research Letters*, **33**, 2–7.
- Piao S, Yin G, Tan J et al. (2015) Detection and attribution of vegetation greening trend in China over the last 30 years. *Global Change Biology*, **21**, 1601–1609.
- Pinzon J, Tucker C (2014) A non-stationary 1981-2012 AVHRR NDVI3g time series.

 *Remote Sensing, 6, 6929–6960.
- Prentice IC, Meng T, Wang H, Harrison S, Ni J, Wang G (2011) Evidence of a universal scaling relationship for leaf CO2 drawdown along an aridity gradient. *New Phytologist*, **190**, 169–180.
- Roerink G, Menenti M, Verhoef W (2000) Reconstructing cloudfree NDVI composites using Fourier analysis of time series. *International Journal of Remote Sensing*, **21**, 1911–1917.
- Ryu Y, Baldocchi D, Kobayashi H et al. (2011) Integration of MODIS land and atmosphere products with a coupled-process model to estimate gross primary productivity and evapotranspiration from 1 km to global scales. *Global Biogeochemical Cycles*, **25**, GB4017.
- Samanta A, Ganguly S, Hashimoto H et al. (2010) Amazon forests did not green-up during the 2005 drought. *Geophysical Research Letters*, **37**, 1–5.
- Sanchez-Lorenzo A, Wild M, Brunetti M et al. (2015) Reassessment and update of long-term trends in downward surface shortwave radiation over Europe (1939-2012). *Journal of Geophysical Research: Atmospheres*, **120**, 9555–9569.

Seddon AWR, Macias-Fauria M, Long PR, Benz D, Willis KJ (2016) Sensitivity of global

terrestrial ecosystems to climate variability. *Nature*, **531**, 229–232.

- Sellers P, Meeson B, Hall F et al. (1995) Remote sensing of the land surface for studies of global change: Models algorithms experiments. *Remote Sensing of Environment*, **51**, 3–26.
- Shabanov N, Huang D, Yang W et al. (2005) Analysis and optimization of the MODIS leaf area index algorithm retrievals over broadleaf forests. *IEEE Transactions on Geoscience and Remote Sensing*, **43**, 1855–1865.
- Stoffelen A (1998) Toward the true near-surface wind speed: Error modeling and calibration using triple collocation. *Journal of Geophysical Research*, **103**, 7755–7766.
- Tian F, Fensholt R, Verbesselt J, Grogan K, Horion S, Wang Y (2015) Evaluating temporal consistency of long-term global NDVI datasets for trend analysis. *Remote Sensing of Environment*, **163**, 326–340.
- Tucker C, Pinzon J, Brown M et al. (2005) An extended AVHRR 8-km NDVI dataset compatible with MODIS and SPOT vegetation NDVI data. *International Journal of Remote Sensing*, **26**, 4485–4498.
- Tum M, Günther K, Böttcher M, Baret F, Bittner M, Brockmann C, Weiss M (2016) Global gap-free MERIS LAI time series (2002-2012). *Remote Sensing*, **8**, 1–19.
- Verger A, Filella I, Baret F, Peñuelas J (2016) Vegetation baseline phenology from kilometric global LAI satellite products. *Remote Sensing of Environment*, **178**, 1–14.
- Vermote E, Justice C, Bréon F (2009) Towards a generalized approach for correction of the BRDF effect in MODIS directional reflectances. *IEEE Transactions on Geoscience and Remote Sensing*, **47**, 898–908.

- Wang M (2009) Ensemble Empirical Mode Decomposition. *Advances in Adaptive Data*Analysis, 1, 1–41.
- Wang D, Morton D, Masek J et al. (2012) Impact of sensor degradation on the MODIS NDVI time series. *Remote Sensing of Environment*, **119**, 55–61.
- Wu Z, Huang NE, Long SR, Peng C-K (2007) On the trend, detrending, and variability of nonlinear and nonstationary time series. *Proceedings of the National Academy of Sciences*, **104**, 14889–14894.
- Xiao Z, Liang S, Wang J, Chen P, Yin X, Zhang L, Song J (2014) Use of General Regression
 Neural Networks for Generating the GLASS Leaf Area Index Product From Time-Series
 MODIS Surface Reflectance. *IEEE Transactions on Geoscience and Remote Sensing*,
 52, 209–223.
- Xiao Z, Liang S, Wang J, Xiang Y, Zhao X, Song J (2016) Long-time-series global land surface satellite leaf area index product derived from MODIS and AVHRR surface reflectance. *IEEE Transactions on Geoscience and Remote Sensing*, **54**, 5301–5318.
- Yan H, Yu Q, Zhu Z-C, Myneni RB, Yan H-M, Wang S-Q, Shugart HH (2013) Diagnostic analysis of interannual variation of global land evapotranspiration over 1982-2011:

 Assessing the impact of ENSO. *Journal of Geophysical Research: Atmospheres*, **118**, 8969–8983.
- Yan K, Park T, Yan G et al. (2016) Evaluation of MODIS LAI/FPAR product Collection 6.

 Part 1: Consistency and improvements. *Remote Sensing*, **8**, 359.
- Yuan H, Dai Y, Xiao Z, Ji D, Shangguan W (2011) Reprocessing the MODIS Leaf AreaIndex products for land surface and climate modelling. *Remote Sensing of Environment*,115, 1171–1187.

- Yuan W, Cai W, Xia J et al. (2014) Global comparison of light use efficiency models for simulating terrestrial vegetation gross primary production based on the LaThuile database. *Agricultural and Forest Meteorology*, **192–193**, 108–120.
- Zhang Y, Song C, Band LE, Sun G, Li J (2017) Reanalysis of global terrestrial vegetation trends from MODIS products: Browning or greening? *Remote Sensing of Environment*, **191**, 145–155.
- Zhou J, Jia L, Menenti M (2015) Reconstruction of global MODIS NDVI time series:

 Performance of Harmonic ANalysis of Time Series (HANTS). *Remote Sensing of Environment*, **163**, 217–228.
- Zhu Z, Bi J, Pan Y et al. (2013) Global data sets of vegetation leaf area index (LAI)3g and fraction of photosynthetically active radiation (FPAR)3g derived from global inventory modeling and mapping studies (GIMMS) normalized difference vegetation index (NDVI3G) for the period 1981 to 2. *Remote Sensing*, **5**, 927–948.
- Zhu Z, Piao S, Myneni R et al. (2016) Greening of the Earth and its drivers. *Nature Climate Change*, **6**, 791–795.
- Zhu Z, Piao S, Lian X, Myneni RB, Peng S, Yang H (2017) Attribution of seasonal leaf area index trends in the northern latitudes with "optimally" integrated ecosystem models.

 Global Change Biology, 1–16.

Table 1. Summary of global satellite LAI products.

	Product	Time span*	Data source	Spatial resolution	Temporal resolution	Reference	
	GLASS	1982–2014	NOAA/AVHRR LTDR reflectance & Terra/MODIS C5 reflectance	0.05°, 1982–1999 1 km, 2001–2011	8-day	(Xiao et al., 2016)	
	GLOBMAP	1982–2011	GIMMS NDVI & Terra/MODIS C5 reflectance	1/13.75°	biweekly, 1982–1999/2 8-day, 2000/3–2011	(Liu et al., 2012)	
	LAI3g	1982-2011	GIMMS NDVI3g	1/12°	bi-weekly	(Zhu et al., 2013)	
	TCDR	1982–2015	NOAA/AVHRR TCDR reflectance	0.05°	daily	(Claverie et al., 2016)	
	GEOV1	1999–2013	SPOT/VGT reflectance	1/112°	10-day	(Baret et al., 2013)	
	MERIS	2003–2011	ENVISAT/MERIS reflectance	1/360°	10-day	(Tum et al., 2016)	
	MODIS C5	2001–2015	Terra/MODIS C5 reflectance	1 km	8-day	(Shabanov et al., 2005)	
	MODIS C6	2001–2015	Terra/MODIS C6 reflectance	500 m	8-day	(Yan et al., 2016)	

*Years with year-round data.

Table 2. Global linear trends, interannual variabilities, uncertainties, and relative uncertainties for different LAI products during different time periods. Bold type indicates a significance level of p<0.05 for linear trends. SD denotes standard deviation.

Product	Linear trend (m ² m ⁻² decade ⁻¹)			Interannual variability (m² m² year¹)		Relative uncertainty (%)			Relative uncertainty variation (%)	
	1982– 2011	1982– 1999	2003– 2011	1982– 2011	1982– 1999	2003- 2011	1982– 2011	1982– 1999	2003- 2011	1982– 2011
GLASS	0.128	0.115	-0.044	0.064	0.074	0.011	11.7	13.3	8.8	3.5
GLOBMAP	-0.026	0.026	-0.098	0.017	0.017	0.014	19.6	19.6	19.5	1.1
LAI3g	0.049	0.082	0.151	0.047	0.057	0.013	8.5	8.1	9.3	2.0
TCDR	0.059	0.057	0.004	0.023	0.027	0.013	13.0	13.6	12.1	1.6
Average	0.053	0.070	0.003	0.038	0.044	0.013	13.2	13.6	12.4	2.1
SD	0.063	0.038	0.107	0.022	0.027	0.001	4.7	4.7	4.9	0.9
GEOV1			0.072			0.013			6.4	_
MERIS			0.049			0.010			14.0	
MODIS C6			0.048			0.008			13.6	
Average			0.056			0.010			11.4	
SD			0.014			0.003			4.3	
MODIS C5		·	-0.019		·	0.011				

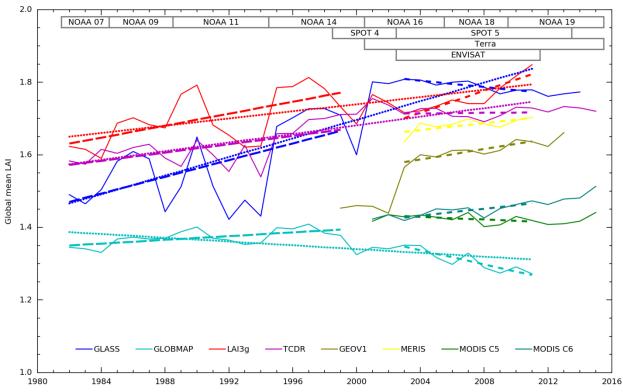
Figure captions

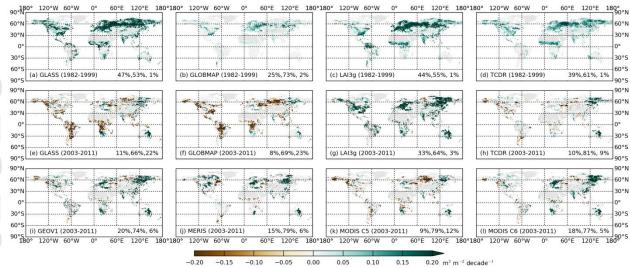
- Fig. 1. Global mean LAI (solid curves) and linear trends during 1982–2011 (dotted lines), 1982–1999 (long dashed lines) and 2003–2011 (short dashed lines) for different LAI products. Trend values are listed in Table 2. Lifespans of different satellite platforms are also illustrated.
- Fig. 2. Linear trend maps of the growing season mean LAI for different LAI products during different time periods. Trends with $p \ge 0.1$ were assigned a value of 0 for illustrative purposes. The three numbers in each subplot indicate the area percentages of positive, zero, and negative trends on vegetated land surface.
- Fig. 3. Global mean LAI, adaptive trends detected by the EEMD method, and detrended anomalies (m² m⁻² year⁻¹). Anomalies (solid curves in b) are the subtraction of adaptive trends (dashed curves in a) from global mean LAI values (solid curves in a). Lifespans of different satellite platforms are also illustrated.
- Fig. 4. Interannual variability maps of growing season mean LAI for different LAI products during different time periods.
- Fig. 5. Uncertainties and relative uncertainties of global mean LAI for different LAI products.
- Fig. 6. Average maps of (a) uncertainty and (b) relative uncertainty of growing season mean LAI for the four long-term LAI products.
- Fig. 7. Average maps of (a) uncertainty variation and (b) relative uncertainty variation of growing season mean LAI for the four long-term LAI products.
- Fig. 8. Linear relationships (a) between relative uncertainty variation over 30 years and the intra-inconsistency index (ratio of interannual variability (IAV) during 1982–1999 to that

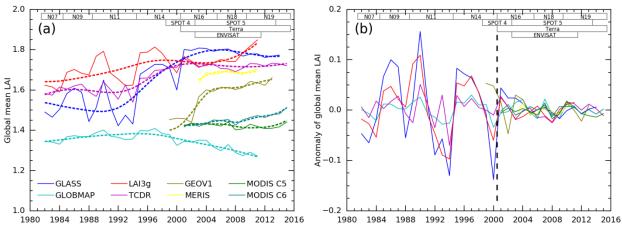
during 2003–2011), and (b) between linear trends and interannual variabilities during the pre-MODIS period (1982–1999), for global values and several big ecosystems. ENF: evergreen needleleaf forest; EBF: evergreen broadleaf foreset; DBF: deciduous broadleaf forest; WSA: woody savanna; GRA: grasslands; CRO: croplands.

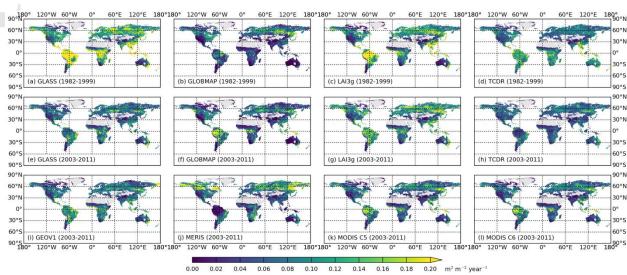
Fig. 9. Agreement of GLASS, GLOBMAP, LAI3g and TCDR on the signs of linear trends during (a) the pre-MODIS period (1982–1999) and (b) the overlap period (2003–2011). Domination refers to at least three of four products agreeing with each other. Significance: p <0.1.

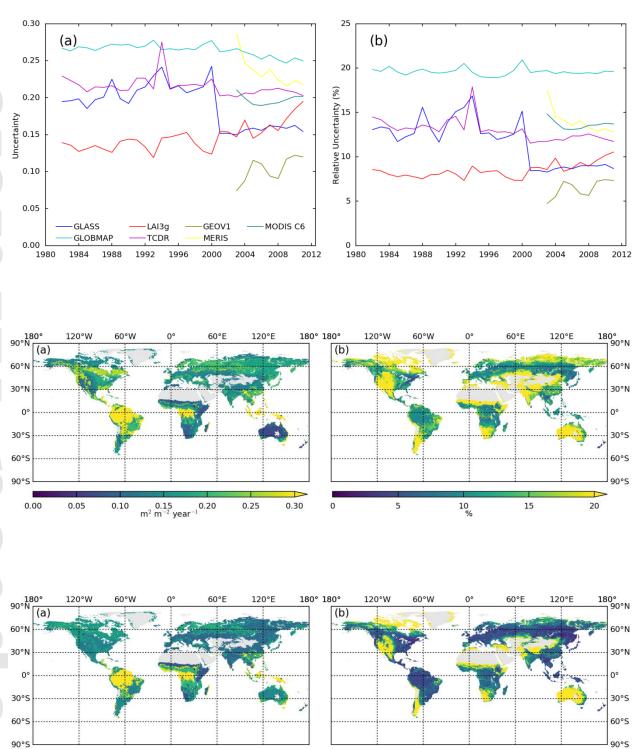
Fig. 10. Mean R^2 maps between detrended anomalies of the four long-term LAI products during (a) the pre-MODIS period (1982–1999) and (b) the overlap period (2003–2011).











10

8

 $0.04 \atop \text{m}^2 \ \text{m}^{-2} \ \text{year}^{-1}$

0.08

0.10

0.02

0.00



